Dynamical correlation effects in a weakly correlated material: Inelastic x-ray scattering and photoemission spectra of beryllium

Azimatu Seidu,[1] Andrea Marini,[2,3] and Matteo Gatti[4,3,5]

[1]*Department of Physics, School of Physical and Mathematical Sciences, College of Basic and Applied Sciences, University of Ghana, Legon, Accra, Ghana*

[2]*Istituto di Struttura della Materia of the National Research Council and Division of Ultrafast Processes in Materials (FLASHit), Via Salaria Km 29.3, I-00016 Monterotondo Stazione, Italy*

[3]*European Theoretical Spectroscopy Facility (ETSF)*

[4]*Laboratoire des Solides Irradiés, École Polytechnique, CNRS, CEA, Université Paris-Saclay, F-91128 Palaiseau, France*

[5]*Synchrotron SOLEIL, L'Orme des Merisiers, Saint-Aubin, BP 48, F-91192 Gif-sur-Yvette, France*

(Received 22 December 2017; published 26 March 2018)

Beryllium is a weakly correlated simple metal. Still we find that dynamical correlation effects, beyond the independent-particle picture, are necessary to successfully interpret the electronic spectra measured by inelastic x-ray scattering (IXS) and photoemission spectroscopies (PES). By combining *ab initio* time-dependent density-functional theory (TDDFT) and many-body Green's function theory in the GW approximation (GWA), we calculate the dynamic structure factor, the quasiparticle (QP) properties and PES spectra of bulk Be. We show that band-structure effects (i.e., due to interaction with the crystal potential) and QP lifetimes (LT) are both needed in order to explain the origin of the measured double-peak features in the IXS spectra. A quantitative agreement with experiment is obtained only when LT are supplemented to the adiabatic local-density approximation (ALDA) of TDDFT. Besides the valence band, PES spectra display a satellite, a signature of dynamical correlation due to the coupling of QPs and plasmons, which we are able to reproduce thanks to the combination of the GWA for the self-energy with the cumulant expansion of the Green's function.

DOI: 10.1103/PhysRevB.97.125144

I. INTRODUCTION

Among the simple metals, beryllium is the one with the highest electronic density [1]. This means that the kinetic energy is expected to dominate over the potential energy and that the Coulomb interaction can be treated as a small perturbation of the ideal Fermi gas. At the same time, the largely covalent bonding and the layered crystal structure (hence intrinsically anisotropic) make beryllium one of the simple metals where the effects of the crystal potential are the most relevant [2,3]. Therefore beryllium is a case study where the independent-particle band-structure picture should most ideally be valid.

Also in view of its apparent simplicity, Be has often served as a prototype material for the experimental development of electron spectroscopy. For example, angle-resolved photoemission spectroscopy [4–15] (ARPES) has brought out its unusual surface electronic properties, which are at the origin of phenomena like acoustic plasmons [16,17] and giant Friedel oscillations [18]. Only very recently, band-structure calculations have provided a rationale for these findings in terms of topologically protected nontrivial surface states originating from a Dirac node line state [19]. Moreover, being a low-Z material, Be has been also a system of choice for Compton [20–25] and inelastic x-ray scattering [26–31] (IXS) experiments. On the one hand, from the determination of the ground-state electron momentum density, Compton scattering provides the characterization of the Fermi surface and electron correlation effects. On the other hand, at low momentum transfers $\mathbf{q}$, IXS identifies the dispersion of plasmons, i.e., collective charge excitations due to the long-range Coulomb interaction, and of other neutral electronic excitations through the measurement of the dynamic structure factor as a function of $\mathbf{q}$.

Here we will use beryllium as a testbed for assessing the theoretical description of electronic excitations that is obtained from the combination of two *ab initio* frameworks such as time-dependent density-functional theory [32] (TDDFT) and many-body perturbation theory [33] (MBPT). In particular, we will address the origin of the double-peak features that characterize the IXS spectra [30] and of the satellites measured in photoemission experiments [34,35]. In both cases, we will discuss the limitations of state-of-the-art approximations such as the adiabatic local-density approximation [36,37] (ALDA) of TDDFT and the GW approximation [38] (GWA) of MBPT. We will show that the solution to their shortcomings can be found in terms of dynamical correlation effects that are beyond a simple independent-particle band-structure picture. As a result of our analysis, it will turn out that dynamical correlation plays a key role even for a weakly correlated material like beryllium.

The rest of the paper is organized as follows. Section II contains a concise summary of the theoretical approach[1] that is needed to understand the results of the calculations, which are discussed in Sec. III. There we analyze in details both IXS (in Secs. III A and III C) and photoemission spectra (in Sec. III B). Finally, Sec. IV contains a summary and the conclusions.

[1]For an extended introduction to the theoretical formalism see Ref. [47].

II. THEORETICAL FRAMEWORK AND COMPUTATIONAL DETAILS

IXS measures the dynamic structure factor [39] $S(\mathbf{q},\omega)$ that in a bulk crystal (in atomic units) can be expressed as

$$S(\mathbf{q}=\mathbf{q}_r+\mathbf{G},\omega) = -\frac{q^2}{4\pi^2 n}\mathrm{Im}\epsilon_M^{-1}(\mathbf{q},\omega) = -\frac{1}{\pi n}\mathrm{Im}\chi_{\mathbf{G},\mathbf{G}}(\mathbf{q}_r,\omega). \quad (1)$$

Here, $\mathbf{q}_r$ belongs to the first Brillouin zone, $\mathbf{G}$ is a reciprocal-lattice vector, n is the mean electron density, ϵ_M the macroscopic dielectric function, and χ is the density-density response function [40].

Within TDDFT [41] χ is calculated from the solution of the Dyson-like equation:

$$\chi_{\mathbf{G},\mathbf{G}'}(\mathbf{q}_r,\omega) = \chi^0_{\mathbf{G},\mathbf{G}'}(\mathbf{q}_r,\omega) + \sum_{\mathbf{G}_1,\mathbf{G}_2}\chi^0_{\mathbf{G},\mathbf{G}_1}(\mathbf{q}_r,\omega) \times\left[v_c(\mathbf{q}_r+\mathbf{G}_1)\delta_{\mathbf{G}_1,\mathbf{G}_2}+f^{\mathrm{xc}}_{\mathbf{G}_1,\mathbf{G}_2}(\mathbf{q}_r,\omega)\right]\chi_{\mathbf{G}_2,\mathbf{G}'}(\mathbf{q}_r,\omega), \quad (2)$$

where χ^0 is the Kohn-Sham (KS) independent-particle response function, v_c is the Coulomb interaction, and f_{xc} is the exchange-correlation kernel. χ^0 contains the band-structure information, since it is built from the KS orbitals $\varphi_{n\mathbf{k}}$ and eigenvalues $\varepsilon_{n\mathbf{k}}$ as (here $f_{n\mathbf{k}}$ are the Fermi occupation numbers, Ω the volume, and $\eta\to 0^+$):

$$\chi^0_{\mathbf{G},\mathbf{G}'}(\mathbf{q}_r,\omega) = \frac{1}{\Omega}\sum_{n,n',\mathbf{k}}\frac{f_{n\mathbf{k}}-f_{n'\mathbf{k}+\mathbf{q}_r}}{\omega+\varepsilon_{n\mathbf{k}}-\varepsilon_{n'\mathbf{k}+\mathbf{q}_r}+i\eta} \times\langle\varphi_{n\mathbf{k}}|e^{-i(\mathbf{q}_r+\mathbf{G})\mathbf{r}}|\varphi_{n'\mathbf{k}+\mathbf{q}_r}\rangle\langle\varphi_{n'\mathbf{k}+\mathbf{q}_r}|e^{+i(\mathbf{q}_r+\mathbf{G}')\mathbf{r}'}|\varphi_{n\mathbf{k}}\rangle. \quad (3)$$

The f_{xc} kernel, which is in principle nonlocal in space and frequency dependent (i.e., dynamical), has to be approximated. While the random-phase approximation (RPA) corresponds to setting $f_{\mathrm{xc}}=0$ in Eq. (2), the ALDA f_{xc} kernel, which is local and static, is the derivative of the KS LDA exchange-correlation potential V_{xc} with respect to the density [36].

To a first approximation [42], angle-integrated photoemission spectroscopy (PES) determines the total spectral function $A(\omega)$, which is the trace of the imaginary part of the one-particle Green's function G:

$$A(\omega)=\sum_{n\mathbf{k}}A_{n\mathbf{k}}(\omega)=\frac{1}{\pi}\sum_{n\mathbf{k}}|\mathrm{Im}G_{n\mathbf{k}}(\omega)|. \quad (4)$$

G can be obtained as a solution of a Dyson equation in terms of the KS independent-particle G^0 and the self-energy Σ_{xc} (we omit the indexes for simplicity):

$$G=G^0+G^0(\Sigma_{\mathrm{xc}}-V_{\mathrm{xc}})G. \quad (5)$$

A popular approximation for the self-energy is Hedin's GWA [38]: $\Sigma_{\mathrm{xc}}=GW$, which is a convolution in frequency space between the Green's function G and the screened Coulomb interaction:

$$W_{\mathbf{G},\mathbf{G}'}(\mathbf{q}_r,\omega)=\epsilon^{-1}_{\mathbf{G},\mathbf{G}'}(\mathbf{q}_r,\omega)v_c(\mathbf{q}_r+\mathbf{G}'). \quad (6)$$

The microscopic dielectric function ϵ is directly linked to response function χ:

$$\epsilon^{-1}_{\mathbf{G},\mathbf{G}'}(\mathbf{q}_r,\omega)=\delta_{\mathbf{G},\mathbf{G}'}+v_c(\mathbf{q}_r+\mathbf{G})\chi_{\mathbf{G},\mathbf{G}'}(\mathbf{q}_r,\omega). \quad (7)$$

In the GWA, χ is generally calculated at the level of the RPA. In the present work, we will compare GW results with ϵ^{-1} obtained from both the RPA and the ALDA.

In the first-order perturbative G_0W_0 scheme [43,44], the GW self-energy is built using KS eigenvalues and orbitals. Assuming that G is diagonal in the KS basis and combining Eqs. (4) and (5), one has

$$A_{n\mathbf{k}}(\omega)=\frac{1}{\pi}\frac{\left|\mathrm{Im}\Sigma^{\mathrm{xc}}_{n\mathbf{k}}(\omega)\right|}{\left[\omega-\varepsilon_{n\mathbf{k}}-\mathrm{Re}\Sigma^{\mathrm{xc}}_{n\mathbf{k}}(\omega)+V^{\mathrm{xc}}_{n\mathbf{k}}\right]^2+\left[\mathrm{Im}\Sigma^{\mathrm{xc}}_{n\mathbf{k}}(\omega)\right]^2}. \quad (8)$$

At the energies that are solution of the equation

$$\omega-\varepsilon_{n\mathbf{k}}-\mathrm{Re}\Sigma^{\mathrm{xc}}_{n\mathbf{k}}(\omega)+V^{\mathrm{xc}}_{n\mathbf{k}}=0, \quad (9)$$

and if correspondingly $\mathrm{Im}\Sigma^{\mathrm{xc}}_{n\mathbf{k}}(\omega)$ is not too large, the spectral function, Eq. (8), displays prominent peaks. The condition (9) defines the energies of the quasiparticle (QP) excitations, which have a finite lifetime that is given by the inverse of $\mathrm{Im}\Sigma^{\mathrm{xc}}_{n\mathbf{k}}$. By a frequency linearization of (9), we have that the QP energies are obtained from

$$\mathrm{Re}E_{n\mathbf{k}}=\varepsilon_{n\mathbf{k}}+\mathrm{Re}Z_{n\mathbf{k}}\left[\mathrm{Re}\Sigma^{\mathrm{xc}}_{n\mathbf{k}}(\varepsilon_{n\mathbf{k}})-V^{\mathrm{xc}}_{n\mathbf{k}}\right] \quad (10)$$

with the renormalization factor Z defined as

$$Z^{-1}_{n\mathbf{k}}=1-\left.\frac{\partial\Sigma_{n\mathbf{k}}(\omega)}{\partial\omega}\right|_{\omega=\varepsilon_{n\mathbf{k}}}. \quad (11)$$

The QP energies, Eq. (10), form the band structure of the material, while Z defines the spectral weight that can be attributed to the QP excitation.

In addition to the QP peaks, the spectral function (8) can have other structures, i.e., satellites, which are a direct consequence of the frequency dependence of the self-energy. In the GWA, Σ_{xc} is the sum of the static and real Fock term Σ_x, which accounts for exchange effects, and the correlation contribution $\Sigma_c(\omega)$, which is dynamical and complex. In the Hartree-Fock approximation, where $\Sigma_c(\omega)$ is 0, the QP excitations have an infinite lifetime and $Z=1$: the spectral function (8), being normalized to 1, is just a δ peak. The origin of other structures in (8) hence stems entirely from the GWA correlation contribution:

$$\Sigma^c_{n\mathbf{k}}(\omega)=\sum_{n'\mathbf{k}',s\neq 0}\frac{\left|W^s_{n\mathbf{k},n'\mathbf{k}'}\right|^2}{\omega-\varepsilon_{n'\mathbf{k}'}+(\omega_s-i\eta)\mathrm{sgn}(\mu-\varepsilon_{n'\mathbf{k}'})}, \quad (12)$$

which is the result of the frequency convolution between the Green's function $G(\omega)$ and $W(\omega)-v_c$. For the details of the derivation we refer to Ref. [42]. The expression in Eq. (12) can be understood as a sum of electron-boson coupling terms [42], where the bosonic excitations ω_s are the plasmon and many-body electron-hole excitations that correspond to the peaks of the dynamic structure factor (1) and the matrix elements $W^s_{n\mathbf{k},n'\mathbf{k}'}$ define their coupling with the electrons.

While the GWA is the state-of-the-art method for QP band structures [45,46], it is known [45,47] to be problematic for satellites. Rather than as a solution of the Dyson equation (5), the Green's function (for an occupied state of energy $\varepsilon_{n\mathbf{k}}$ smaller than the Fermi level μ) can be alternatively obtained

from the exponential [48] of the cumulant function $C_{n\mathbf{k}}(t)$:

$$G_{n\mathbf{k}}(\omega) = \frac{i}{2\pi}\int_{-\infty}^{0} dt e^{i[\omega-(\varepsilon_{n\mathbf{k}}+\Sigma^{x}_{n\mathbf{k}}-V^{\mathrm{xc}}_{n\mathbf{k}})]t} e^{C_{n\mathbf{k}}(t)}. \quad (13)$$

Merged with the GWA into the GW+C scheme [49], the cumulant function is obtained from

$$C_{n\mathbf{k}}(t) = \frac{1}{\pi}\int_{-\infty}^{\mu-\varepsilon_{n\mathbf{k}}} d\omega\left(\frac{i\omega t - 1 + e^{-i\omega t}}{\omega^2}\right) \times \mathrm{Im}\left[\Sigma^{\mathrm{xc}}_{n\mathbf{k}}(\omega+\varepsilon_{n\mathbf{k}})\right]. \quad (14)$$

In Eq. (14), the first term in the fraction numerator represents the correlation contribution to the QP correction of the KS energy, Eq. (10). The second term gives the corresponding renormalization factor, while the last exponential term produces a series of satellites at energies ω_s away from the QP peak. For recent discussions about the cumulant Green's function formalism, we refer to Refs. [50–52].

In the present work, we have adopted a plane-wave pseudopotential approach, using a norm-conserving pseudopotential from Ref. [53]. Ground-state properties, calculated in the local-density approximation (LDA) of KS density functional theory were obtained with a kinetic energy cutoff of 25 Ry. For the loss-function calculations, we used a $48\times48\times24$ **k**-point grid, which was reduced to $24\times24\times12$ for GW calculations. We included 30 bands in the sum over states (3) and 40 bands in (12). The $\epsilon^{-1}_{\mathbf{G},\mathbf{G}'}$ matrix (7) had a 35 **G**-vector size. Finally, the convolution between G and W to obtain the GW self-energy was performed numerically by sampling the real-axis integration with 135 frequencies. We note that, in order to avoid inconsistencies [38,54,55] between the KS energies entering Σ_{xc} and the excitation energies in the spectral function, the self-energy should be calculated in an energy-self-consistent scheme rather than within G_0W_0 or at least following the procedure of Fermi level alignment suggested by Hedin [38,42]. However, in the present case, these procedures can be avoided as the G_0W_0 corrections (<0.2 eV) to KS energies are very small compared to the plasmon energies of Be (∼18 eV). We have used QUANTUM ESPRESSO [56] and ABINIT [57] for KS ground-state calculations, DP [58] for the simulation of IXS spectra, YAMBO [59] for GW, and the CUMUPY cumulant code [60] for spectral function calculations in the GW+C scheme.

III. RESULTS AND DISCUSSION

A. Dynamic structure factor: RPA and ALDA

Early IXS experiments [27] on Be (and at the same time also on Al and graphite) found, quite unexpectedly, that at large momentum transfers the dynamic structure factor $S(\mathbf{q},\omega)$ exhibits a peculiar peak-and-shoulder or double-peak structure, showing deviations from the RPA predictions on the homogeneous electrons gas (HEG). The speculation about those structures being the possible signature of an incipient Wigner crystallization triggered an intense debate. Strong correlation effects of the HEG at large **q** (i.e., at short range in real space), where the RPA is not adequate, were firstly invoked [61–67]. Later on, also on the basis of the strong angular dependence of the double-peak structures [29,30], it was recognized that their origin was rather to be ascribed to the band structure of the materials (i.e., to the interaction with the crystal potential) through the presence of gaps in the unoccupied density of states (DOS) [68,69]. Pioneering *ab initio* RPA simulations [70], on the basis of the real electronic structure of Be, were instrumental in reaching this conclusion. More recently, there have been other calculations of the plasmon dispersion [31,71], also in comparison with measurements on polycrystalline samples [31], however, the fine structures in the IXS data [29,30] have not been reexamined with present-day computational capabilities.

Figure 1 presents the comparison between the available experimental IXS data from Ref. [30] (grey dots) and the dynamic structure factor $S(\mathbf{q},\omega)$ that we have calculated both in the RPA (violet curves) and the ALDA (yellow curves), as a function of momentum transfer **q** (of increasing size from bottom to top panels) along 3 different directions in the reciprocal space. At the smallest momentum transfer, a prominent peak is visible in the spectra for the three directions, corresponding to the valence plasmon resonance of Be around 20 eV. The agreement between experiment and calculations is very good, with the ALDA that slightly improves over the RPA. By increasing **q**, the small shoulder on the high-energy side of the main peak develops as a second structure. In the experiment, the first peak maintains the largest intensity, whereas in the calculations the second structure is always a sharp peak, whose intensity, even though direction dependent, is much larger than in the experiment when compared to the first peak. The ALDA gives a better agreement with experiment, especially at large momentum transfers and for energies smaller than ∼20 eV, by shifting the spectral weight to lower energies with respect to the RPA. However, in the experiment, the spectrum at large **q** is characterized by a rather broad particle-hole continuum band, while in the calculated spectra, sharp and dispersing peaks are always superimposed on a continuous background.

The origin of these peaks is in the band structure, and more precisely in the electron-hole excitations, which are visible also in the RPA, thus confirming the interpretation [29,30,70] that the fine structures in the IXS spectra are due to the material properties and do not derive from the universal properties of the electron-electron interaction in metals. At the same time, the static exchange-correlation contribution contained in the ALDA is not sufficient to get a quantitative agreement with experiment: those band-structure-related features remain always too strong in the calculations. We will come back to this point in Sec. III C, after having examined in the next section the effects of dynamical correlation beyond the independent-particle band-structure picture, by comparing MBPT calculations with experimental PES spectra.

B. Photoemission spectra: quasiparticles and satellites from the GWA and beyond

Figure 2 shows the band structure of beryllium calculated using both the LDA KS eigenvalues $\varepsilon_{n\mathbf{k}}$ and the GW QP energies $\mathrm{Re}(E_{n\mathbf{k}})$ obtained by using Eq. (10). The first fully occupied band is parabolic, with the bottom at the Γ point. The Fermi level crosses less dispersive bands in the ΓKM plane but not in the parallel AHL, where a large gap opens instead. This gives rise to a dip in the DOS (not shown) near

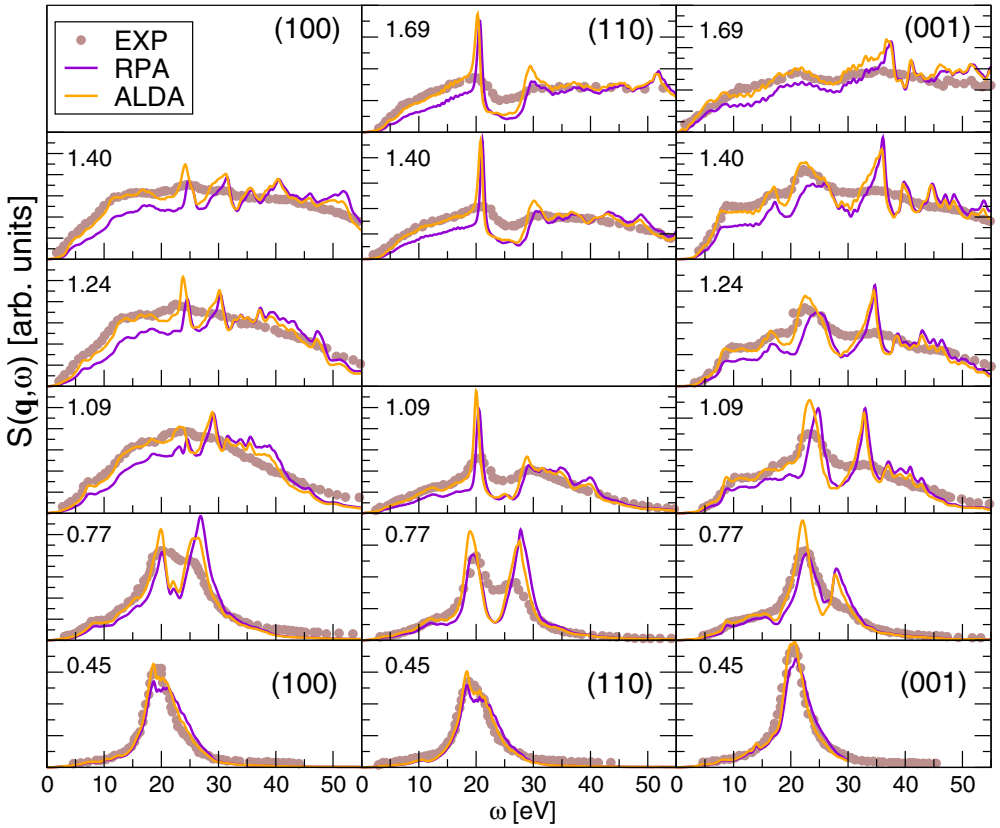

FIG. 1. IXS experimental data of Be from Ref. [30] (grey dots) are compared with dynamic structure factors $S(\mathbf{q},\omega)$ calculated in the RPA (violet curves) and the ALDA (orange curves). Spectra are shown for three different directions in the reciprocal space, from the left to the right, and for increasing momentum transfers going from bottom to top panels. The value of the momentum transfer (in atomic units) is reported in the top-left corner of each panel. Two panels are left blank since the corresponding experimental data are missing in Ref. [30]. Arbitrary units are used everywhere for $S(\mathbf{q},\omega)$.

the Fermi level, making Be almost similar to a semimetal. The linear-band crossings, at the Fermi level in the $M\Gamma$ direction and just above along ΓK, have been recently identified as a sign of the occurrence of a Dirac node line [19].

The GW corrections are always small: the differences $[\mathrm{Re}(E_{n\mathbf{k}}) - \varepsilon_{n\mathbf{k}}]$ [see Eq. (10)] are in most cases smaller than 0.2 eV (see Fig. 3). The GW narrowing of the valence bandwidth in Be is negligible, in contrast to GW results for other simple metals and the HEG [38,72–74]. Also the quite

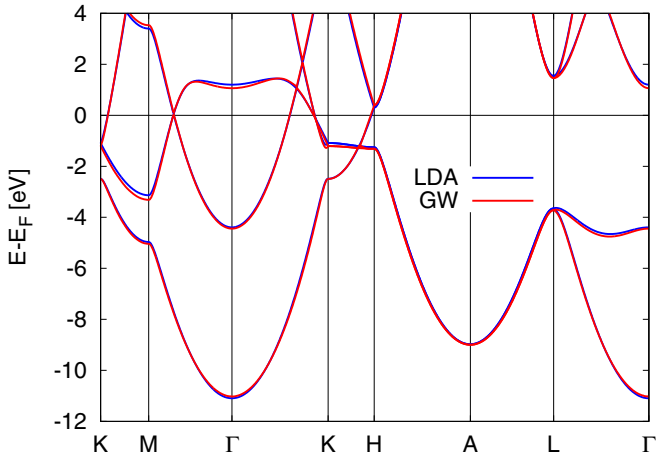

FIG. 2. Comparison between the LDA and the GW band structure along a path in the hexagonal Brillouin zone of Be. Here and in the other figures in this section, the zero of the energy axis is set at the Fermi level.

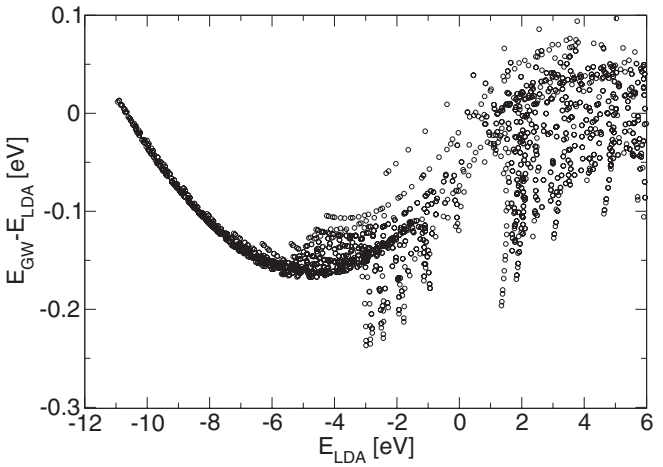

FIG. 3. GW corrections $\mathrm{Re}E_{n\mathbf{k}} - \varepsilon_{n\mathbf{k}}$ as a function of the LDA eigenvalues $\varepsilon_{n\mathbf{k}}$.

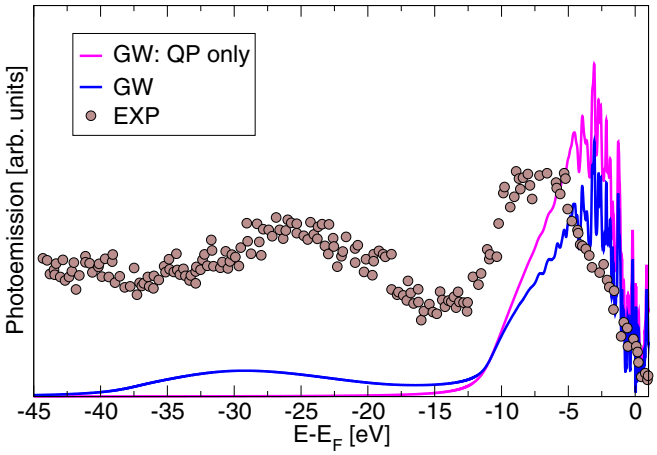

FIG. 4. Quasiparticle-only (purple curve) and full GW (blue curve) spectral functions compared with experimental photoemission data with photon energy $h\nu = 1486$ eV from Ref. [34]. Here and in the following comparisons with the photoemission experiment, the spectra are in arbitrary units.

large renormalization factors $\mathrm{Re}(Z_{n\mathbf{k}})$ [see Eq. (11)], which are $\sim$0.65 for the first band but larger than 0.7 for the others, confirm that beryllium is a weakly correlated metal. The GW binding energies of the first and second bands at the Γ point are 10.9 and 4.4 eV, which are in good agreement with the experimental ARPES values [4], 11.1 ± 0.1 and 4.8 ± 0.1 eV, respectively.[2] Our GW QP band structure hence also supports the conclusions of Ref. [19], which were based on an LDA band structure.

If we calculate the spectral function in the QP approximation,

$$A(\omega) = \frac{1}{\pi} \sum_{n\mathbf{k}} \frac{\left|\mathrm{Im}\Sigma^{\mathrm{xc}}_{n\mathbf{k}}(\varepsilon_{n\mathbf{k}})\right|}{\left[\omega - \varepsilon_{n\mathbf{k}} - \mathrm{Re}\Sigma^{\mathrm{xc}}_{n\mathbf{k}}(\varepsilon_{n\mathbf{k}}) + V^{\mathrm{xc}}_{n\mathbf{k}}\right]^2 + \left[\mathrm{Im}\Sigma^{\mathrm{xc}}_{n\mathbf{k}}(\varepsilon_{n\mathbf{k}})\right]^2}, \quad (15)$$

we obtain the purple curve in Fig. 4. In comparison with experimental (angle-integrated) PES data [34], see the grey dots in Fig. 4, we find that the QP valence band corresponds to the first broad peak in the experiment, ranging from the Fermi level to $\sim$11 eV binding energy. In the calculation, there are more sharp peaks and the overall profile of the valence band peak is quite different from experiment: we will come back to this point. The most notable qualitative difference is, however, the fact that the experimental data show other structures with larger binding energies, which are completely absent in the QP-only spectral function.

In order to understand these additional features, we need to calculate the full GW spectral function [see Eq. (8)], which, besides the valence band, indeed also displays a broad satellite (see blue curve in Fig. 4). However, the satellite in GW is still not in very good agreement with experiment: it has a different shape and its center of mass is located at too large binding energies, with a discrepancy of several eV with respect to experiment. This is a typical shortcoming of the GWA, found in several other simple metals and semiconductors [49,75–78], which is ascribed to the GW prediction of an experimentally nonexistent plasmaron excitation [50,51,79–81].

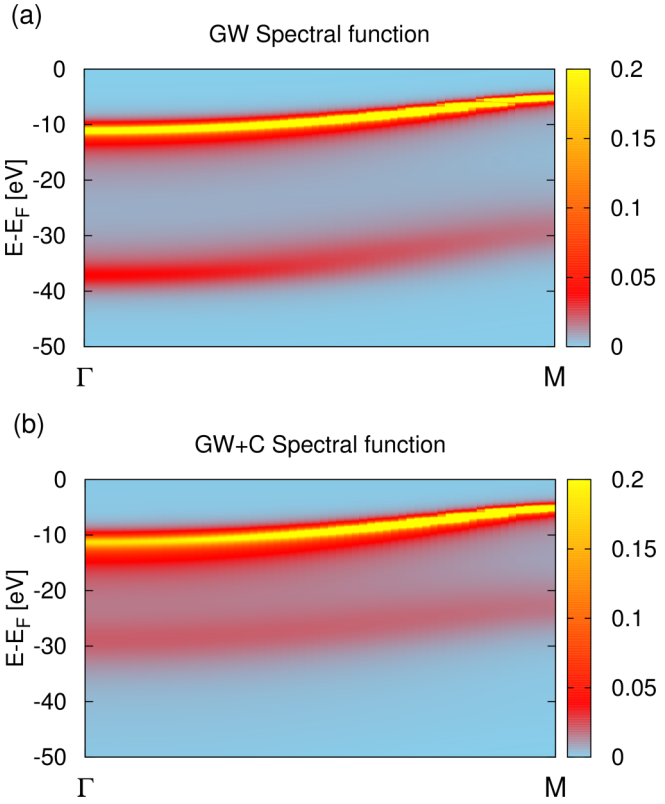

FIG. 5. (a) GW and (b) GW+C spectral functions $A_{n\mathbf{k}}(\omega)$ for the first Be band along the ΓM direction.

To track more closely the origin of this GW drawback in Be, in Fig. 5, we compare the GW and GW+C spectral functions $A_{n\mathbf{k}}(\omega)$ for the first band along the ΓM direction. The most intense parabolic line in the color plots, dispersing from -11 to -5 eV going from Γ to M, corresponds to the lowest QP band of Fig. 2. The differences between GW and GW+C results concern the rest of the spectrum, where in both cases there is only one additional satellite, at variance with other simple metals like Na where a series of satellites is instead generally found [35,49,51]. In GW, the satellite along ΓM disperses from -37 to -29 eV, i.e., at a distance from the QP peak that varies from 28 to 24 eV while moving to smaller binding energies. Instead, in $GW + \mathrm{C}$ the distance between the QP and the satellite, which is broader than in GW, is constantly $\sim$18 eV. This value matches well the plasmon energy at $\mathbf{q} \to 0$ that is experimentally estimated to be equal to 18–19 eV [82–85]. This demonstrates that the satellite in the PES spectra originates from the coupling between the QP and the valence plasmon. The satellite dispersion in Be qualitatively resembles that of the HEG [86,87]. However, quantitative deviations from the HEG results are found already for Na [88], which is the

[2]Also electron momentum spectroscopy experiments find similar values [84].

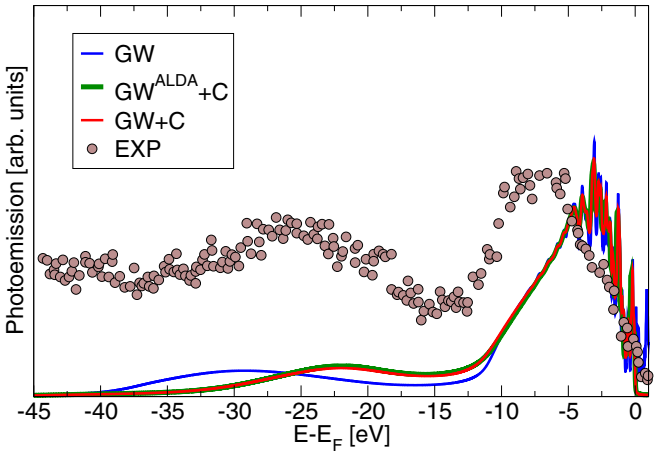

FIG. 6. GW (blue curve), GW+C (red curve), and $GW^{\mathrm{ALDA}}+\mathrm{C}$ (green curve) spectral functions compared with experimental photoemission data with photon energy $h\nu = 1486$ eV from Ref. [34].

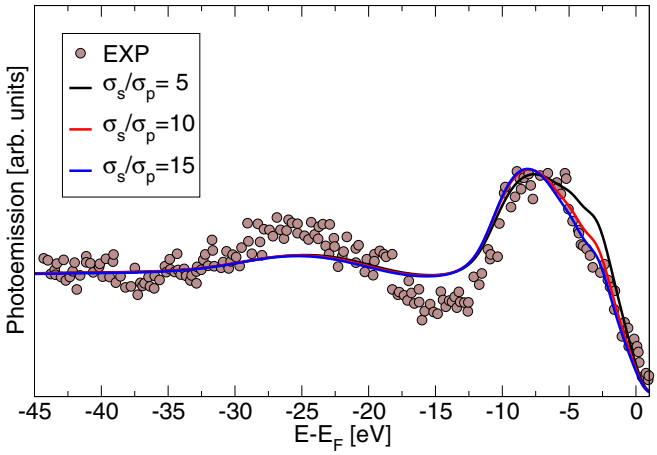

FIG. 7. Photoemission spectra simulated from the GW+C spectral function $A(\omega)$—see Fig. 6—as a function of photoexcitation cross section ratio σ_s/σ_p for $2s$ and $2p$ states, with inclusion of a Shirley background and convoluted with experimental resolution of 0.6 eV, in comparison with experimental photoemission data from Ref. [34].

closest realisation of the HEG. In Be the effect of the crystal potential is much larger and so are the deviations from the HEG.

Turning to the total spectral functions (summed over bands and $\mathbf{k}$ points), in Fig. 6, we see that in the comparison with the PES experiment the GW+C result (red curve) improves considerably the plasmon-satellite position over the GWA (blue curve). This satellite in Be is a broad feature in the spectrum ($\sim$15 eV wide), since in addition to the first parabolic band (analysed in detail in Fig. 5) also the second band at smaller binding energies contributes to it.

In Sec. III A, we have shown that the ALDA gives dynamic structure factors in better agreement with IXS experimental data than the RPA, which is the level of approximation also used in standard GW and GW+C calculations of spectral functions. The question that naturally arises is then whether electron-hole interactions beyond the RPA also affect the spectral function. We have therefore calculated the dynamically screened Coulomb interaction W also using the dielectric function from the ALDA, as input for obtaining GW+C spectral functions. The result of this $GW^{\mathrm{ALDA}}+\mathrm{C}$ calculation is hardly visible in Fig. 6 (green curve) as it overlaps almost entirely with the GW+C (red curve), which is based on the RPA. On the one hand, this finding clarifies that in Be the determination of W for spectral-function calculations is adequate already at the RPA level. On the other hand, we can explain this result by noting that, while different at large wave vectors, the RPA and ALDA $S(\mathbf{q},\omega)$ are very similar at small $\mathbf{q}$ (for example, see the bottom panel in Fig. 1). This in turn implies (as recently shown also for sodium [88]) that in simple metals (where the electrons are delocalized) the small-wave-vector components $\mathbf{q}\sim 0$ of the dielectric function are those that give the most important contributions to the self-energy [which is in principle a sum of all components, see Eq. (12)].

Even though the energy position of all the spectral features from the GW+C calculation match well the experiment, there are still important discrepancies in their intensities. This indicates that even an accurate calculation of the spectral function is not sufficient to get a quantitative agreement with photoemission spectra. A clear evidence of this statement is the fact that photoemission spectra are generally photon-energy dependent (for an example covering a large photon-energy range see Ref. [89]), while spectral functions are not. Here we consider the photon-energy dependence of the photoemission process (which would require a rather involved treatment [90]) only on a qualitative level. One ingredient is the inclusion of the photoemission cross sections, which, to a first approximation, usually can be taken from tables of calculated atomic photoionization cross sections [91,92]. However, the valence atomic configuration of Be is $2s$, while in the solid a large amount of valence electrons have $2p$ character due to the hybridization of the $2s$ and $2p$ states [3]. As a consequence, the photoemission cross sections cannot be evaluated in the standard way [93]. In Refs. [34,35] from a fit to the experimental data, the ratio of the s to p photoexcitation cross sections was estimated as $\sigma_s/\sigma_p = 5$. Here we are interested to see how the spectra change as a function of this cross section ratio, which partly simulates the effect of photon-energy dependence. We have then convoluted the resulting spectra with a Gaussian of 0.6 eV to take into account the experimental resolution [34,35] and added a Shirley background for "secondary electrons" [93,94]. They are electrons that are excited by the photoexcited electrons (i.e., the "primary electrons") and are also able to reach the detector giving an additional contribution to the measured total photocurrent. For additional details, we refer to Ref. [95].

Considering the rough procedure that we have followed here, the agreement of the calculated photoemission spectra with experiment in Fig. 7 is very good. Concerning the valence band, by increasing the relative weight of $2s$ states (i.e., by increasing σ_s/σ_p), the shoulder at ~ -2 eV, which has the largest $2p$ contribution, gets progressively damped, confirming that the experimental spectrum at $h\nu = 1486$ eV photon energy is mainly probing $2s$ states [34,35]. On the other side, even by varying the cross sections σ_s/σ_p, the intensity of the satellite remains always underestimated with respect to the main QP

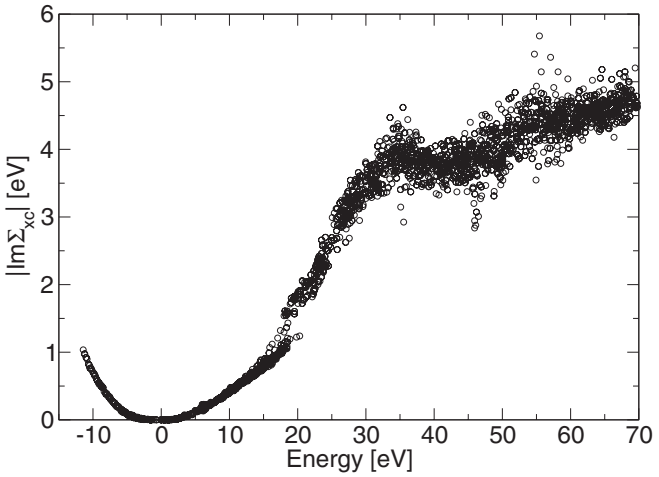

FIG. 8. Absolute value of the imaginary part of the self-energy $|\mathrm{Im}\Sigma^{\mathrm{xc}}|$ calculated in the GWA as a function of energy (the Fermi level is set at 0). The QP lifetime for holes (negative energies) and electrons (positive energies) is the inverse of $|\mathrm{Im}\Sigma^{\mathrm{xc}}|$.

peak. This is consistent with the fact that the so-called extrinsic and interference effects [90] here are not included in the simulation. While escaping from the sample, the photoelectron can still induce additional excitations in the system (losing partly its kinetic energy), which are called extrinsic contributions to distinguish them from the excitations induced by the photohole. The latter are instead called intrinsic as they are contained in the spectral function $A(\omega)$ of the system. The two contributions can additionally interfere, leading to a third interference term [90]. In the present case, we can conclude that extrinsic and interference effects indeed give a nonnegligible contribution to the measured Be spectra, giving more weight to the satellite part. An advanced treatment of the photoemission process would be required to get a quantitative description, which is beyond the scope of the present work. Here the agreement with experiment is sufficiently good to safely confirm the plasmonic origin of the satellite in Be and the ability of the GW+C approach to describe it.

C. Dynamic structure factor: lifetime effects

Taking the point of view of MBPT, the TDDFT kernel simulates both the self-energy corrections to the KS eigenvalues and the electron-hole interaction [96–99]. Especially at large momentum transfers [100], the two contributions partially cancel each other in such a way that the ALDA has to reproduce the remaining short-range effects. However, the real and static ALDA does not contain the damping of neutral excitations due to their interaction with multiple electron-hole pairs, which would require a dynamical and complex kernel. Following previous TDDFT calculations on Si, Na, and Al [101–104], (which were also inspired by pioneering works on the HEG [61,66,105]), here we assume that the main effect beyond ALDA is due to the finite lifetime of holes and electrons and we neglect further corrections due to the electron-hole interaction.

Within the GWA, the quasiparticles have a finite lifetime since the self-energy is complex and dynamical. Figure 8 shows the imaginary part of the GW self-energy matrix–elements—whose inverse yield the QP lifetime—over a wide energy range. In agreement with previous GW calculations[3] on Be [71,106,107], we find that at energies close to the Fermi level (i.e., the 0 of the energy axis in Fig. 8), $|\mathrm{Im}\Sigma^{\mathrm{xc}}|$ has the parabolic behavior typical of a Fermi liquid [108]. For higher energies, the material-specific band structure affects significantly the results showing large deviations from a simple parabola. We note that for energies that are 10–15 eV far from the Fermi energy, $|\mathrm{Im}\Sigma^{\mathrm{xc}}|$ for both holes and electrons is as large as 1 eV and increases up to 4–5 eV for electrons of energies 30 eV above the Fermi level. These large values at energies comparable to the plasmon energy of beryllium are a hint that lifetime effects can play an important role in the calculation of the dynamic structure factor.

Since there is no available TDDFT kernel that efficiently includes lifetime effects, we take the pragmatic approach of Refs. [101–104] and replace the imaginary $i\eta$ in the denominator of χ_0 [see Eq. (3)] by $i|\mathrm{Im}\Sigma^{\mathrm{xc}}_{n\mathbf{k}}| + i|\mathrm{Im}\Sigma^{\mathrm{xc}}_{n'\mathbf{k}+\mathbf{q}_r}|$. In practice, we retain only the energy dependence of $|\mathrm{Im}\Sigma^{\mathrm{xc}}(\omega)|$ by making a numerical fit of the GW results (Fig. 8). In the Dyson equation (2), we then consider both the RPA and ALDA kernels.

The dynamic structure factors $S(\mathbf{q},\omega)$ obtained with the inclusion of lifetime (LT) effects are shown in Fig. 9. The main action of LTs is to wash out all the sharp peaks present in the spectra calculated without them (see Fig. 1). This brings the ALDA+LT (red curves) in very good agreement with experiment [30] (grey dots), keeping the same improvement over RPA+LT (blue curves) already discussed in Sec. III A. For the largest momentum transfers, we just observe a small underestimation of the ALDA+LT spectra with respect to experiment, as LTs lead to an overbroadening at large energies, which was similarly found for the other materials in Refs. [101–104]. A possible reason for this too large LT effect could be due to vertex corrections [109,110], which are neglected here.

All in all, we can safely conclude that the fine structures observed in IXS experiments [27,29,30] can be explained as a combined result of band-structure properties of Be, which for unoccupied states differ from the HEG, and finite QP lifetimes, which are a manifestation of the electron-electron interaction. The consideration of the band structure only leads to a drastic overestimation of those features (see Fig. 1), while the simultaneous inclusion of lifetimes in ALDA calculation is the key to accurately reproduce the experimental data [30].

IV. SUMMARY

Beryllium is a prototypical weakly correlated metal. Indeed, if we confine our analysis to its quasiparticle (QP) properties only, we find that GW corrections to the LDA band structure are small (less than 0.2 eV) and that both the LDA and the GWA are in good agreement with available experimental data (within the uncertainty linked to the analysis of ARPES experiments). However, if we extend our study to a broader perspective, the satellite characterizing the photoemission valence spectrum requires to go beyond a QP picture, since it is the signature of dynamical correlation given by the coupling of

[3]For other lifetime calculations in simple metals see, e.g., Refs. [111–113].

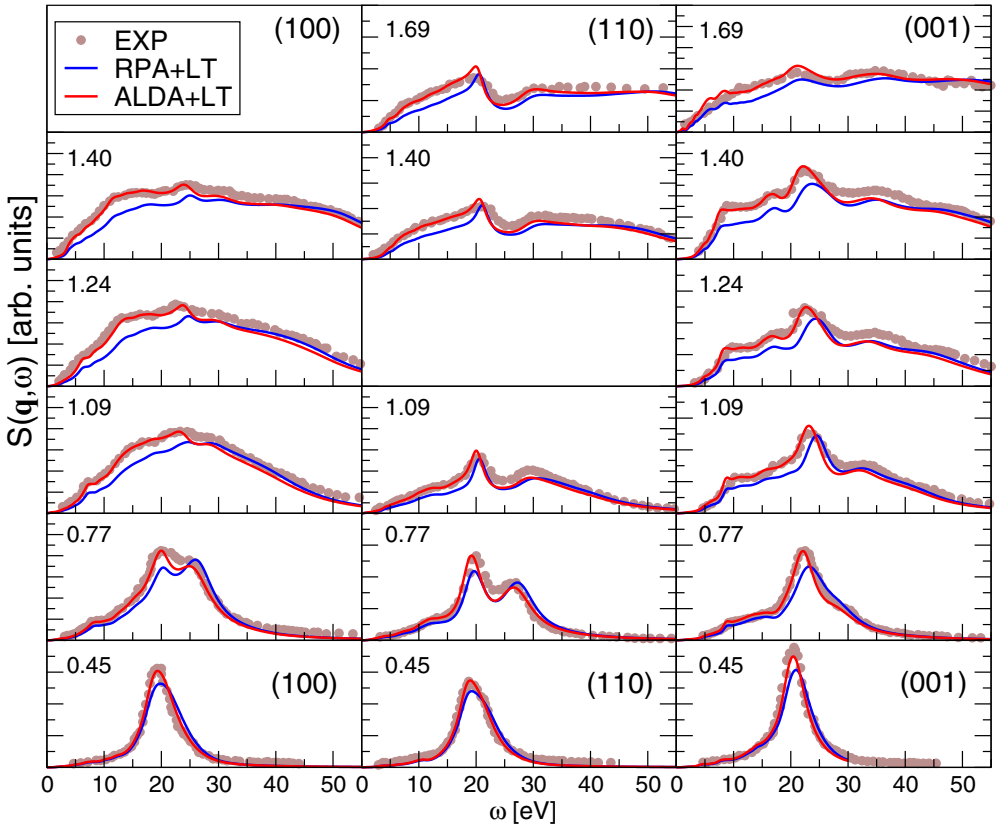

FIG. 9. IXS experimental data of Be from Ref. [30] (grey dots) are compared with dynamic structure factors $S(\mathbf{q},\omega)$ calculated in the RPA+LT (blue curves) and the ALDA+LT (red curves) schemes. See also Fig. 1 where quasiparticle lifetimes (LT) are not considered.

two kinds of elementary excitations, the QPs and the plasmons. In order to correctly interpret this plasmon satellite, even in Be the GWA is not sufficient. To overcome this limitation, we have combined the GWA with the cumulant expansion of the Green's function into the GW+C scheme, which is needed in order to capture efficiently the physics of plasmon satellites, as recently shown also in other materials.

Considering IXS data, we have found that the ALDA, which is the workhorse of TDDFT, is not able to accurately reproduce the measured spectra. Instead, we have shown that only the simultaneous consideration of band-structure effects and quasiparticle lifetimes explains the origin of the double peaks in the spectra, a feature that has been debated for long time.

In summary, our results bring forward the essential role of dynamical correlation effects (related to the frequency dependence of Σ_{xc}) also for the electronic excitation properties of a simple metal like beryllium, whose correct description requires to go beyond state-of-the-art approximations of *ab initio* methods like the GWA and the ALDA.

ACKNOWLEDGMENTS

We acknowledge the African School on Electronic Structure: Methods and Applications (ASESMA) where this work was initiated. AS also thanks Lucia Reining and the Palaiseau Theoretical Spectroscopy Group for the kind hospitality. This research was supported by a Marie Curie FP7 Integration Grant within the 7th European Union Framework Programme. Computational time was granted by GENCI (Project No. 544). AM acknowledges the funding received from the European Union project MaX *Materials design at the eXascale* H2020-EINFRA-2015-1, Grant Agreement No. 676598 and *Nanoscience Foundries and Fine Analysis - Europe* H2020-INFRAIA-2014-2015, Grant Agreement No. 654360.

[1] N. Ashcroft and N. Mermin, *Solid State Physics* (Holt, Rinehart and Winston, 1976).
[2] S. ichi T. Inoue and J. Yamashita, J. Phys. Soc. Jpn. **35**, 677 (1973).
[3] M. Y. Chou, P. K. Lam, and M. L. Cohen, Phys. Rev. B **28**, 4179 (1983).
[4] E. Jensen, R. A. Bartynski, T. Gustafsson, E. W. Plummer, M. Y. Chou, M. L. Cohen, and G. B. Hoflund, Phys. Rev. B **30**, 5500 (1984).
[5] E. Jensen, R. A. Bartynski, T. Gustafsson, and E. W. Plummer, Phys. Rev. Lett. **52**, 2172 (1984).
[6] R. A. Bartynski, E. Jensen, T. Gustafsson, and E. W. Plummer, Phys. Rev. B **32**, 1921 (1985).
[7] M. Hengsberger, D. Purdie, P. Segovia, M. Garnier, and Y. Baer, Phys. Rev. Lett. **83**, 592 (1999).
[8] M. Hengsberger, R. Frésard, D. Purdie, P. Segovia, and Y. Baer, Phys. Rev. B **60**, 10796 (1999).

[9] S. LaShell, E. Jensen, and T. Balasubramanian, Phys. Rev. B **61**, 2371 (2000).

[10] T. Balasubramanian, L. I. Johansson, P. A. Glans, C. Virojanadara, V. M. Silkin, E. V. Chulkov, and P. M. Echenique, Phys. Rev. B **64**, 205401 (2001).

[11] S.-J. Tang, J. Shi, B. Wu, P. T. Sprunger, W. L. Yang, V. Brouet, X. J. Zhou, Z. Hussain, Z.-X. Shen, Z. Zhang, and E. W. Plummer, Physica Status Solidi (b) **241**, 2345 (2004).

[12] I. Vobornik, J. Fujii, M. Mulazzi, G. Panaccione, M. Hochstrasser, and G. Rossi, Phys. Rev. B **72**, 165424 (2005).

[13] I. Vobornik, J. Fujii, M. Hochstrasser, D. Krizmancic, C. E. Viol, G. Panaccione, S. Fabris, S. Baroni, and G. Rossi, Phys. Rev. Lett. **99**, 166403 (2007).

[14] T. Y. Chien, E. D. L. Rienks, M. F. Jensen, P. Hofmann, and E. W. Plummer, Phys. Rev. B **80**, 241416(R) (2009).

[15] T. Y. Chien, X. He, S.-K. Mo, M. Hashimoto, Z. Hussain, Z.-X. Shen, and E. W. Plummer, Phys. Rev. B **92**, 075133 (2015).

[16] V. M. Silkin, A. García-Lekue, J. M. Pitarke, E. V. Chulkov, E. Zaremba, and P. M. Echenique, Europhys. Lett. **66**, 260 (2004).

[17] B. Diaconescu, K. Pohl, L. Vattuone, L. Savio, P. Hofmann, V. M. Silkin, J. M. Pitarke, E. V. Chulkov, P. M. Echenique, D. Farias, and M. Rocca, Nature (London) **448**, 57 (2007).

[18] P. T. Sprunger, L. Petersen, E. W. Plummer, E. Lægsgaard, and F. Besenbacher, Science **275**, 1764 (1997).

[19] R. Li, H. Ma, X. Cheng, S. Wang, D. Li, Z. Zhang, Y. Li, and X.-Q. Chen, Phys. Rev. Lett. **117**, 096401 (2016).

[20] K. Hämäläinen, S. Manninen, C.-C. Kao, W. Caliebe, J. B. Hastings, A. Bansil, S. Kaprzyk, and P. M. Platzman, Phys. Rev. B **54**, 5453 (1996).

[21] M. Itou, Y. Sakurai, T. Ohata, A. Bansil, S. Kaprzyk, Y. Tanaka, H. Kawata, and N. Shiotani, J. Phys. Chem. Solids **59**, 99 (1998).

[22] S. Huotari, K. Hämäläinen, S. Manninen, S. Kaprzyk, A. Bansil, W. Caliebe, T. Buslaps, V. Honkimäki, and P. Suortti, Phys. Rev. B **62**, 7956 (2000).

[23] S. Huotari, K. Hämäläinen, S. Manninen, C. Sternemann, A. Kaprolat, W. Schülke, and T. Buslaps, Phys. Rev. B **66**, 085104 (2002).

[24] G. Kontrym-Sznajd, M. Samsel-Czekała, S. Huotari, K. Hämäläinen, and S. Manninen, Phys. Rev. B **68**, 155106 (2003).

[25] S. Huotari, C. Sternemann, M. Volmer, J. A. Soininen, G. Monaco, and W. Schülke, Phys. Rev. B **76**, 235106 (2007).

[26] P. Eisenberger, P. M. Platzman, and K. C. Pandy, Phys. Rev. Lett. **31**, 311 (1973).

[27] P. M. Platzman and P. Eisenberger, Phys. Rev. Lett. **33**, 152 (1974).

[28] A. Vradis and G. D. Priftis, Phys. Rev. B **32**, 3556 (1985).

[29] W. Schülke, U. Bonse, H. Nagasawa, S. Mourikis, and A. Kaprolat, Phys. Rev. Lett. **59**, 1361 (1987).

[30] W. Schülke, H. Nagasawa, S. Mourikis, and A. Kaprolat, Phys. Rev. B **40**, 12215 (1989).

[31] G. Tirao, G. Stutz, V. M. Silkin, E. V. Chulkov, and C. Cusatis, J. Phys.: Condens. Matter **19**, 046207 (2007).

[32] E. Runge and E. K. U. Gross, Phys. Rev. Lett. **52**, 997 (1984).

[33] A. Fetter and J. Walecka, *Quantum Theory of Many-particle Systems* (McGraw-Hill, New York, 1971).

[34] H. Höchst, P. Steiner, and S. Hufner, J. Phys. F **7**, L309 (1977).

[35] H. Höchst, P. Steiner, and S. Hüfner, Z. Phys. B **30**, 145 (1978).

[36] A. Zangwill and P. Soven, Phys. Rev. A **21**, 1561 (1980).

[37] E. K. U. Gross and W. Kohn, Phys. Rev. Lett. **55**, 2850 (1985).

[38] L. Hedin, Phys. Rev. **139**, A796 (1965).

[39] W. Schülke, *Electron Dynamics by Inelastic X-Ray Scattering*, Oxford Series on Synchrotron Radiation (Oxford University Press, Oxford, 2007).

[40] G. Onida, L. Reining, and A. Rubio, Rev. Mod. Phys. **74**, 601 (2002).

[41] C. Ullrich, *Time-Dependent Density-Functional Theory: Concepts and Applications*, Oxford Graduate Texts (Oxford University Press, Oxford, 2012).

[42] L. Hedin, J. Phys.: Condens. Matter **11**, R489 (1999).

[43] M. S. Hybertsen and S. G. Louie, Phys. Rev. B **34**, 5390 (1986).

[44] R. W. Godby, M. Schlüter, and L. J. Sham, Phys. Rev. B **37**, 10159 (1988).

[45] F. Aryasetiawan and O. Gunnarsson, Rep. Prog. Phys. **61**, 237 (1998).

[46] M. van Schilfgaarde, T. Kotani, and S. Faleev, Phys. Rev. Lett. **96**, 226402 (2006).

[47] R. Martin, L. Reining, and D. Ceperley, *Interacting Electrons: Theory and Computational Approaches* (Cambridge University Press, Cambridge, 2016).

[48] R. Kubo, J. Phys. Soc. Jpn. **17**, 1100 (1962).

[49] F. Aryasetiawan, L. Hedin, and K. Karlsson, Phys. Rev. Lett. **77**, 2268 (1996).

[50] M. Guzzo, G. Lani, F. Sottile, P. Romaniello, M. Gatti, J. J. Kas, J. J. Rehr, M. G. Silly, F. Sirotti, and L. Reining, Phys. Rev. Lett. **107**, 166401 (2011).

[51] J. S. Zhou, J. J. Kas, L. Sponza, I. Reshetnyak, M. Guzzo, C. Giorgetti, M. Gatti, F. Sottile, J. J. Rehr, and L. Reining, J. Chem. Phys. **143**, 184109 (2015).

[52] B. Gumhalter, V. Kovač, F. Caruso, H. Lambert, and F. Giustino, Phys. Rev. B **94**, 035103 (2016).

[53] M. Lazzeri and S. de Gironcoli, Phys. Rev. B **65**, 245402 (2002).

[54] F. Bruneval and M. Gatti, Top. Curr. Chem. **347**, 99 (2014).

[55] M. Gatti, G. Panaccione, and L. Reining, Phys. Rev. Lett. **114**, 116402 (2015).

[56] P. Giannozzi, S. Baroni, N. Bonini, M. Calandra, R. Car, C. Cavazzoni, D. Ceresoli, G. L. Chiarotti, M. Cococcioni, I. Dabo, A. Dal Corso, S. de Gironcoli, S. Fabris, G. Fratesi, R. Gebauer, U. Gerstmann, C. Gougoussis, A. Kokalj, M. Lazzeri, L. Martin-Samos, N. Marzari, F. Mauri, R. Mazzarello, S. Paolini, A. Pasquarello, L. Paulatto, C. Sbraccia, S. Scandolo, G. Sclauzero, A. P. Seitsonen, A. Smogunov, P. Umari, and R. M. Wentzcovitch, J. Phys.: Condens. Matter **21**, 395502 (2009).

[57] X. Gonze, G.-M. Rignanese, M. Verstraete, J.-M. Beuken, Y. Pouillon, R. Caracas, F. Jollet, M. Torrent, G. Zerah, M. Mikami *et al.*, Z. Kristallogr **220**, 558 (2005).

[58] http://www.dp-code.org.

[59] A. Marini, C. Hogan, M. Grüning, and D. Varsano, Comput. Phys. Commun. **180**, 1392 (2009).

[60] J. S. Zhou *et al.* (unpublished).

[61] G. Mukhopadhyay, R. K. Kalia, and K. S. Singwi, Phys. Rev. Lett. **34**, 950 (1975).

[62] H. De Raedt and B. De Raedt, Phys. Rev. B **18**, 2039 (1978).

[63] K. Utsumi and S. Ichimaru, Phys. Rev. B **23**, 3291 (1981).

[64] F. Green, D. N. Lowy, and J. Szymański, Phys. Rev. Lett. **48**, 638 (1982).

[65] K. Awa, H. Yasuhara, and T. Asahi, Phys. Rev. B **25**, 3670 (1982).

[66] S. Rahman and G. Vignale, Phys. Rev. B **30**, 6951 (1984).
[67] F. Green, D. Neilson, and J. Szymański, Phys. Rev. B **31**, 2796 (1985).
[68] W. Schülke, H. Schulte-Schrepping, and J. R. Schmitz, Phys. Rev. B **47**, 12426 (1993).
[69] S. Huotari, C. Sternemann, M. C. Troparevsky, A. G. Eguiluz, M. Volmer, H. Sternemann, H. Müller, G. Monaco, and W. Schülke, Phys. Rev. B **80**, 155107 (2009).
[70] N. E. Maddocks, R. W. Godby, and R. J. Needs, Phys. Rev. B **49**, 8502 (1994).
[71] V. M. Silkin, E. V. Chulkov, and P. M. Echenique, Phys. Rev. B **68**, 205106 (2003).
[72] G. D. Mahan and B. E. Sernelius, Phys. Rev. Lett. **62**, 2718 (1989).
[73] J. E. Northrup, M. S. Hybertsen, and S. G. Louie, Phys. Rev. B **39**, 8198 (1989).
[74] G. D. Mahan and E. W. Plummer, in *Handbook of Surface Science*, edited by K. Horn and M. Scheffler, (Elsevier, Amsterdam, 2000), Vol. 2, pp. 953–987, Chap. 14.
[75] A. S. Kheifets, V. A. Sashin, M. Vos, E. Weigold, and F. Aryasetiawan, Phys. Rev. B **68**, 233205 (2003).
[76] F. Caruso, H. Lambert, and F. Giustino, Phys. Rev. Lett. **114**, 146404 (2015).
[77] F. Caruso and F. Giustino, Phys. Rev. B **92**, 045123 (2015).
[78] J. Lischner, G. K. Pálsson, D. Vigil-Fowler, S. Nemsak, J. Avila, M. C. Asensio, C. S. Fadley, and S. G. Louie, Phys. Rev. B **91**, 205113 (2015).
[79] B. I. Lundqvist, Phys. Kondens. Materie **6**, 193 (1967).
[80] B. I. Lundqvist, Phys. Kondens. Materie **6**, 206 (1967).
[81] J. Lischner, D. Vigil-Fowler, and S. G. Louie, Phys. Rev. Lett. **110**, 146801 (2013).
[82] O. Sueoka, J. Phys. Soc. Jpn. **20**, 2203 (1965).
[83] T. Aiyama and K. Yada, J. Phys. Soc. Jpn. **36**, 1554 (1974).
[84] V. A. Sashin, M. A. Bolorizadeh, A. S. Kheifets, and M. J. Ford, J. Phys.: Condens. Matter **13**, 4203 (2001).
[85] H. Raether, *Excitation of Plasmons and Interband Transitions by Electrons*, Springer Tracts in Modern Physics (Springer, Berlin, Heidelberg, 2006).
[86] F. Caruso and F. Giustino, Eur. Phys. J. B **89**, 238 (2016).
[87] D. Vigil-Fowler, S. G. Louie, and J. Lischner, Phys. Rev. B **93**, 235446 (2016).
[88] J. S. Zhou, M. Gatti, J. J. Kas, J. J. Rehr, and L. Reining, Phys. Rev. B **97**, 035137 (2018).
[89] E. Papalazarou, M. Gatti, M. Marsi, V. Brouet, F. Iori, L. Reining, E. Annese, I. Vobornik, F. Offi, A. Fondacaro, S. Huotari, P. Lacovig, O. Tjernberg, N. B. Brookes, M. Sacchi, P. Metcalf, and G. Panaccione, Phys. Rev. B **80**, 155115 (2009).
[90] L. Hedin, J. Michiels, and J. Inglesfield, Phys. Rev. B **58**, 15565 (1998).
[91] J. H. Scofield, Theoretical Photoionization Cross Sections from 1 to 1500 keV, LLNL Report UCRL-51326, 1973, doi: 10.2172/4545040.
[92] M. Trzhaskovskaya, V. Nefedov, and V. Yarzhemsky, At. Data Nucl. Data Tables **77**, 97 (2001).
[93] M. Guzzo, J. J. Kas, F. Sottile, M. G. Silly, F. Sirotti, J. J. Rehr, and L. Reining, Eur. Phys. J. B **85**, 1 (2012).
[94] D. A. Shirley, Phys. Rev. B **5**, 4709 (1972).
[95] S. Hüfner, *Photoelectron Spectroscopy: Principles and Applications* (Springer, Berlin, 2003).
[96] R. Del Sole, G. Adragna, V. Olevano, and L. Reining, Phys. Rev. B **67**, 045207 (2003).
[97] G. Adragna, R. Del Sole, and A. Marini, Phys. Rev. B **68**, 165108 (2003).
[98] R. Stubner, I. V. Tokatly, and O. Pankratov, Phys. Rev. B **70**, 245119 (2004).
[99] F. Bruneval, F. Sottile, V. Olevano, R. Del Sole, and L. Reining, Phys. Rev. Lett. **94**, 186402 (2005).
[100] F. Iori, F. Rodolakis, M. Gatti, L. Reining, M. Upton, Y. Shvyd'ko, J.-P. Rueff, and M. Marsi, Phys. Rev. B **86**, 205132 (2012).
[101] H.-C. Weissker, J. Serrano, S. Huotari, F. Bruneval, F. Sottile, G. Monaco, M. Krisch, V. Olevano, and L. Reining, Phys. Rev. Lett. **97**, 237602 (2006).
[102] H.-C. Weissker, J. Serrano, S. Huotari, E. Luppi, M. Cazzaniga, F. Bruneval, F. Sottile, G. Monaco, V. Olevano, and L. Reining, Phys. Rev. B **81**, 085104 (2010).
[103] M. Cazzaniga, H.-C. Weissker, S. Huotari, T. Pylkkänen, P. Salvestrini, G. Monaco, G. Onida, and L. Reining, Phys. Rev. B **84**, 075109 (2011).
[104] S. Huotari, M. Cazzaniga, H.-C. Weissker, T. Pylkkänen, H. Müller, L. Reining, G. Onida, and G. Monaco, Phys. Rev. B **84**, 075108 (2011).
[105] T. K. Ng and B. Dabrowski, Phys. Rev. B **33**, 5358 (1986).
[106] I. Campillo, V. M. Silkin, J. M. Pitarke, E. V. Chulkov, A. Rubio, and P. M. Echenique, Phys. Rev. B **61**, 13484 (2000).
[107] I. Y. Sklyadneva, E. V. Chulkov, W.-D. Schöne, V. M. Silkin, R. Keyling, and P. M. Echenique, Phys. Rev. B **71**, 174302 (2005).
[108] G. Giuliani and G. Vignale, *Quantum Theory of the Electron Liquid*, Masters Series in Physics and Astronomy (Cambridge University Press, Cambridge, 2005).
[109] A. Fleszar and W. Hanke, Phys. Rev. B **56**, 10228 (1997).
[110] A. Marini and A. Rubio, Phys. Rev. B **70**, 081103 (2004).
[111] W.-D. Schöne, R. Keyling, M. Bandić, and W. Ekardt, Phys. Rev. B **60**, 8616 (1999).
[112] P. Echenique, J. Pitarke, E. Chulkov, and A. Rubio, Chem. Phys. **251**, 1 (2000).
[113] V. P. Zhukov, E. V. Chulkov, and P. M. Echenique, Phys. Rev. B **72**, 155109 (2005).